ORIGINAL PAPER

Fabrication and Magnetic Properties of Electrospun La$_{0.7}$Sr$_{0.3}$MnO$_3$ Nanostructures

Rattakarn Yensano · Supree Pinitsoontorn · Vittaya Amornkitbamrung · Santi Maensiri

Abstract La$_{0.7}$Sr$_{0.3}$MnO$_3$ (abbreviated as LSMO) nanostructures were fabricated by a simple electrospinning using a solution that contained poly(vinylpyrrolidone) (PVP), lanthanum, strontium and manganese nitrates. The LSMO nanostructures were successfully obtained from calcination of the as-spun LSMO/PVP composite nanofibers at 500–900 °C in air for 7 h. The as-spun and calcined LSMO/PVP composite nanofibers were characterized by X-ray diffraction (XRD), scanning electron microscopy (SEM), and transmission electron microscopy (TEM). Analysis of phase composition by XRD revealed that all the calcined samples have a single rhombohedral LSMO phase. The SEM results showed that the crystal structure and morphology of the LSMO nanofibers were affected by the calcination temperature. Crystallite size of the nanoparticles contained in nanofibers increased with an increase in calcination temperature. The specific saturation magnetization (M_s) values were obtained to be 1.23, 28.61, and 40.52 emu/g at 10 kOe for the LSMO samples calcined respectively at 500, 700, and 900 °C. It is found that the increase of the tendency of M_s is consistent with the enhancement of crystallinity, and the values of M_s for the calcined LSMO samples were observed to increase with increasing crystallite size. This increase in M_s for the calcined LSMO samples with increasing crystallite size may be explained by considering a magnetic domain of the samples.

Keywords Manganite · Electrospinning · Nanofibers · Nanostructures · Magnetic properties

1 Introduction

Perovskite manganites Ln$_{1-x}$A$_x$MnO$_3$ (Ln: trivalent rare-earth ions, A: divalent alkaline-earth ions) have recently attracted much attention due to their interesting physical properties and potential applications [1–3]. Among others, Sr-doped LaMnO$_3$ is particularly of interest due to its good magnetic, electrical and catalytic properties. Sr-doped LaMnO$_3$ with nominal composition La$_{0.7}$Sr$_{0.3}$MnO$_3$ (abbreviated as LSMO) showed a better performance as compared to other compositions and therefore it has become the research focus in this material system: LSMO possesses the highest value of Curie temperature ($T_C = 370$ K) and combines low carrier density (10^{21}–10^{22} cm^{-3}) with a high spin polarization of charge carriers, which makes it very promising in room temperature applications [4, 5]. It also has the largest magnetoresistance (MR) near room temperature and it is already widely recognized that the double exchange (DE) interaction between pairs of Mn^{3+} and Mn^{4+} ions through an oxygen atom is responsible for the ferromagnetic and metallic properties in these manganese oxides [6–8].

Recently, nanocrystalline magnetic materials have received much attention due to their novel material properties that are significantly different from those of their bulk counterparts [9]. The nanostructured magnetic materials such as

R. Yensano · S. Pinitsoontorn · V. Amornkitbamrung
Department of Physics, Faculty of Science, Khon Kaen University, Khon Kaen 40002, Thailand

S. Maensiri (✉)
School of Physics, Institute of Science, Suranaree University of Technology, Nakhon Ratchasima 30000, Thailand
e-mail: santimaensiri@g.sut.ac.th

S. Maensiri
e-mail: santimaensiri@gmail.com

S. Maensiri
NANOTEC-SUT Center of Excellence on Advanced Functional Nanomaterials, Suranaree University of Technology, Nakhon Ratchasima 30000, Thailand

nanorods and nanowires have currently attracted much interest due to their enhanced magnetic property [10, 11]. Nanostructured form of magnetic materials would be of great interest due to their large surface-to-volume ratio, and this expands their technological application in many areas including nanocomposites, nanocatalyts, nanosensors, nanoelectronics and photonics.

Electrospinning represents a simple and convenient method for preparing polymer fibers and ceramic fibers with both solid and hollow interiors that are exceptionally long in length, uniform in diameter ranging from tens of nanometers to several micrometers, and diversified in composition [12–16]. For fabrication of oxide and complex oxide nanostructures by electrospinning, a typical procedure consists of three major steps: (1) preparation of an inorganic sol or a solution containing a polymer together with an alkoxide or salt; (2) electrospinning of the solution to prepare nanofibers of polymer/inorganic composite; (3) calcination of the composite fibers to obtain the desired ceramic nanofibers. In some cases various nanostructures can be fabricated by electrospinning with designed conditions. To date, electrospun magnetic nanofibers and nanostructures of $NiFe_2O_4$ [17], $CoFe_2O_4$ [18], $MnFe_2O_4$ [19], $MgFe_2O_4$ [20], $CuFe_2O_4$ [21], and $ZnFe_2O_4$ [22] have been reported.

Recently, electrospinning has been used to fabricate lanthanum manganite-based nanofibers. Zhou et al. [23] reported the preparation of electrospun polycrystalline lanthanum manganite ($LaMnO_3$) nanofibers of 50–100 nm by calcination of the inorganic/PVA hybrid fibers at 600 °C for 1 h. The morphology, microstructure, crystal structure and thermal analysis were investigated by SEM, TEM, XRD and TG-DSC, respectively. Philip et al. [24] reported the large low-field magnetoresistance in $La_{0.67}Sr_{0.33}MnO_3$ nanowire device. The $La_{0.67}Sr_{0.33}MnO_3$ nanowires were prepared by calcination of the electrospun inorganic/PVP hybrid fibers at 550 °C for 3 h in ultrahigh purity argon and 3 % hydrogen gas mixture. Additional 1 h annealing was carried out in argon and 10 % oxygen atmosphere at 730 °C. The prepared sample was characterized by SEM, Raman, SQUID. It is noted that the specific saturation magnetization (M_s) values of the samples were obtained to be 1×10^{-4} emu/g, which is quite low for Sr-doped lanthanum manganite. Most recently, Zhi et al. [25] reported the preparation of lanthanum strontium manganite ($La_{0.8}Sr_{0.2}MnO_3$) nanofibers by the electrospinning method and annealing at 1050 °C for use as a sensing electrode of an electrochemical sensor with yttria-stabilized zirconia (YSZ) electrolyte for carbon monoxide detection at high temperatures over 500 °C. The electrospun nanofibers form a porous network electrode, which provides a continuous pathway for charge transport. Since the nanofibers possess a higher specific surface area than conventional micron-sized powders, the nanofiber electrode

exhibits a higher electromotive force and better electrocatalytic activity towards CO oxidation. Therefore, the sensor with the nanofiber electrode shows a higher sensitivity, lower limit of detection and faster response to CO than a sensor with a powder electrode.

In this work, we report the fabrication of $La_{0.7}Sr_{0.3}MnO_3$ (LSMO) nanostructures with high M_s by calcination of the electrospun composite nanofibers of lanthanum nitrate/strontium nitrate/manganese nitrate/polyvinylpyrrolidone (PVP). The prepared LSMO nanostructures were well characterized by X-ray diffraction (XRD), scanning electron microscopy (SEM), and transmission electron microscopy (TEM). Magnetic properties of the samples were measured using vibrating sample magnetometry (VSM). The effect of calcination on the morphology, structure, and magnetic properties of the electrospun LSMO nanostructures is investigated.

2 Experimental

To prepare electrospun LSMO nanostructures, lanthanum nitrate, strontium nitrate and manganese nitrate with 0.7: 0.3: 1 molar ratio of La: Sr: Mn was used as starting materials. In a typical procedure, 0.758 g of $LaN_3O_9 \cdot 6H_2O$ (Alfa Aesar) 0.166 g of $Sr(NO_3)_2$ (Beijing Chemical Co. Ltd.) and 0.608 g of $Mn(NO_3)_2 \cdot 4H_2O$ (Beijing Chemical Co. Ltd.) were dissolved in 8 mL of N-Dimethylfumamide (Fluka). The precursor solution was stirred for 12 h, then put it into the 30 mL aqueous PVP (Acros Organics, Mw $\approx$ 90,000) solution of 25 wt.% and subsequently was further stirred for 24 h. The prepared mixed solution was loaded into a plastic syringe equipped with a 22-gauge needle made of stainless steel. The electrospinning process was carried out using our home-made electrospinning system. The schematic diagram of electrospinning process is shown in Fig. 1. The needle was connected to a high-voltage supply and for each solution the voltage of 14.5 kV was applied.
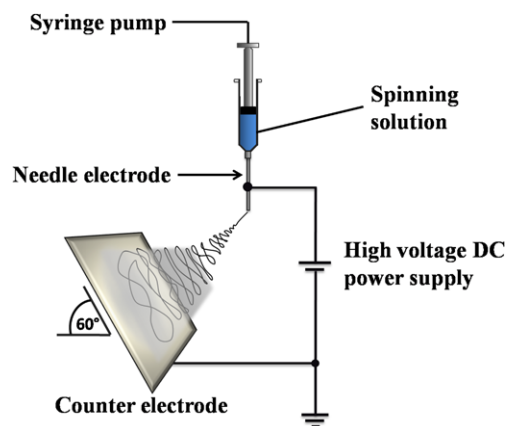

Fig. 1 Schematic diagram of electrospinning setup

The solution was fed at a rate of 0.08 mL/h using a motor syringe pump. A piece of flat aluminum foil was placed 20 cm below the tip of the needle to collect the nanofibers, which was held at 60° horizontal angle, and used to collect the nanofibers. All electrospinning processes were carried out at room temperature.

The electrospun composite nanofibers of PVP/LSMO were calcined at 500, 700, and 900 °C for 7 h in air using heating rates of 5 °C/min. The final products obtained were black LSMO samples. The as-spun and calcined samples were characterized by means of X-ray diffraction (XRD) using $CuK\alpha$ radiation with $\lambda = 0.15418$ nm (Philips PW3040, The Netherlands) and scanning electron microscopy (SEM) (LEO VP1450, U.K. and Hitachi FE-SEM S-4700, Japan). The average diameter of the as-spun composite nanofibers was determined from about 200 measurements. The particle size and morphology of the calcined powders were characterized by transmission electron microscopy (TEM, Hitachi H8100 200 kV).The magnetic properties of the calcined samples were examined at room temperature (20 °C) using a vibrating sample magnetometer (Lake Shore VSM 7403, USA).

3 Results and Discussion

Figure 2 shows morphology and fiber diameter distribution of the as-spun PVP/LSMO composite fibers. Figure 2a is a digital camera photograph showing a sheet of as-prepared fibers taken out from aluminum foil, while Figs. 2b–2e shows the SEM micrographs of the as-spun fibers at magnifications of ×1000 (Fig. 2b) and ×10000 (Fig. 2c) with the respective diameter histograms (Fig. 2e). Each individual nanofiber was quite uniform in cross section, and the average diameter of the fibers was 183 ± 40 nm.

The PVP was selectively removed by calcination of the as-spun PVP/LSMO composite fibers in air above 500 °C [16, 18, 20–22]. Figure 3 shows the SEM micrographs of the LSMO samples calcined at 500, 700, and 900 °C with heating rates of 5 °C/min. It is seen from Fig. 3a that the as-spun composite nanofibers calcined at 500 °C remain as continuous structures, and their diameters are reduced from 183 ± 40 to 160 ± 25 nm. The reduction in size of the nanofibers should be attributed to the loss of PVP from the nanofibers and the crystallization of LSMO. After calcination at 700 and 900 °C (Figs. 3b and 3c), the nature of nanofibers was dramatically changed, and a structure of packed particles or crystallites has become prominent. This is similar to the other complex oxide nanostructures fabricated by electrospinning [14–16, 18, 20–22].

The XRD patterns of the LSMO samples calcined at 500, 700, and 900 °C are shown in Fig. 4. For the calcined samples, all of the main peaks are indexed as the LSMO with rhombohedral structure as shown in the standard data (JCPDS: 51-0409). It is clearly seen that the reflection peaks become sharper and narrower along with the

Fig. 2 Morphology and fiber diameter distribution of the as-spun LSMO/PVP composite sample. (**a**) Digital photograph, (**b**) ×10000 SEM image, (**c**) ×30000 SEM image, (**d**) fiber diameter distribution
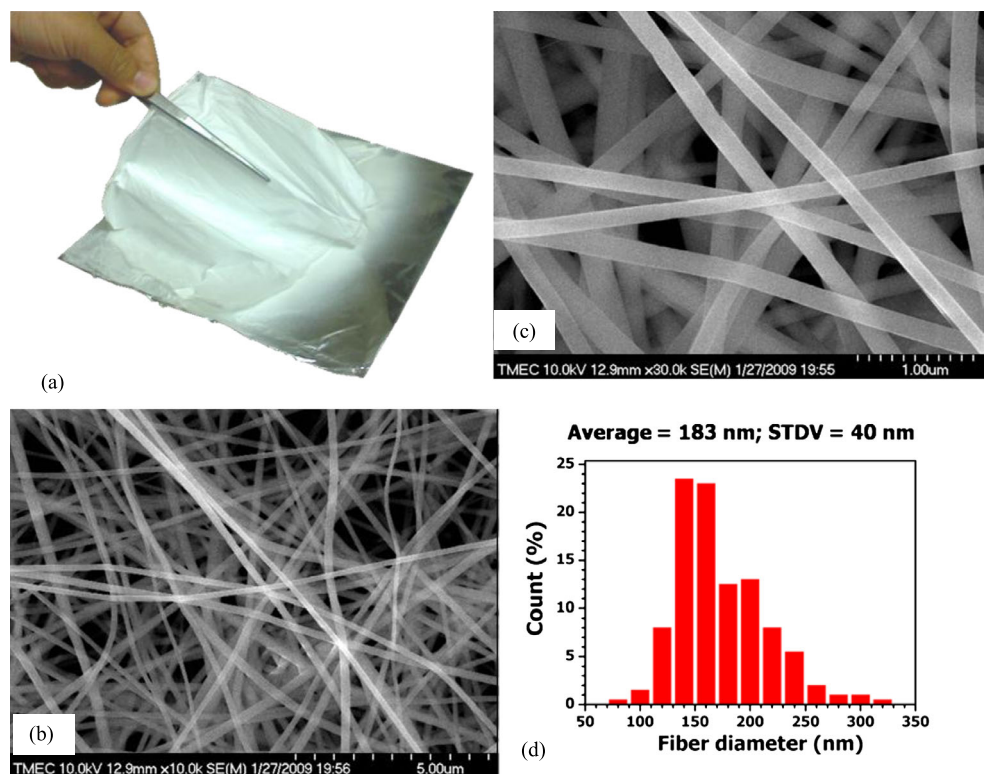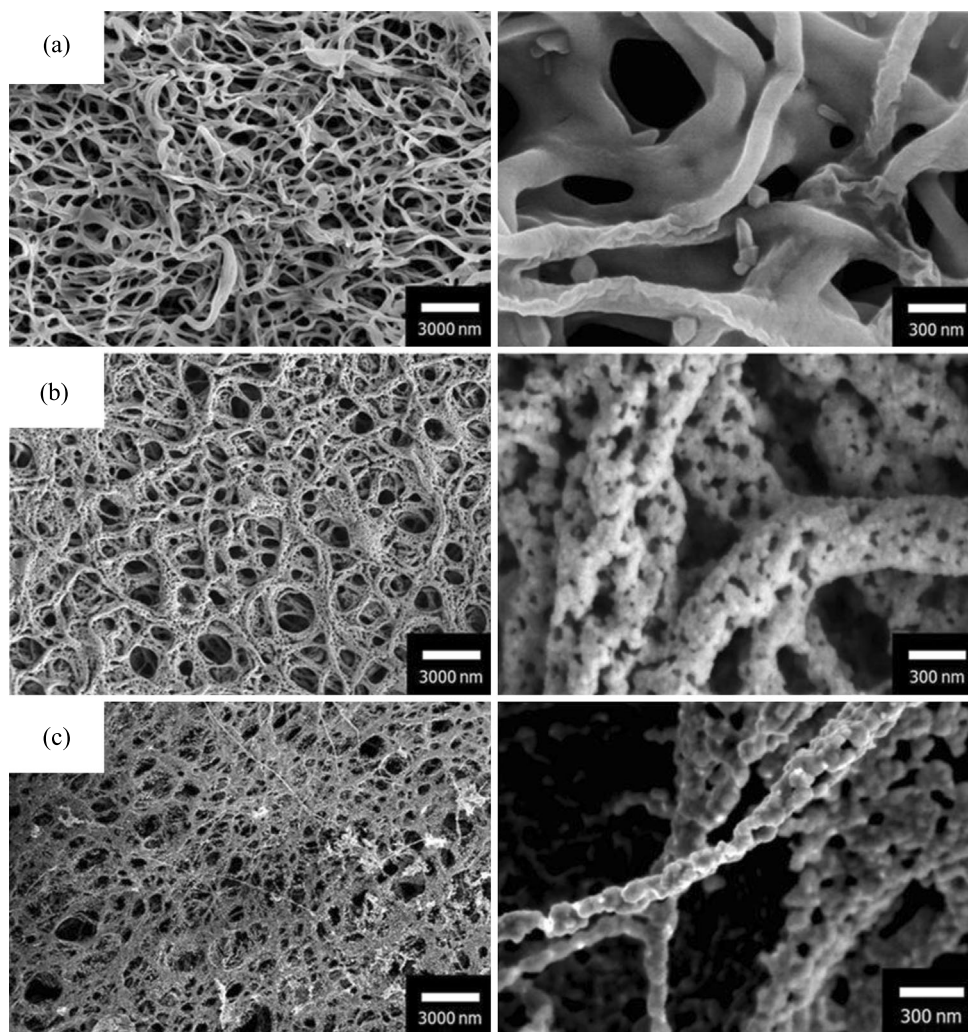
Fig. 3 SEM micrographs of the electrospun LSMO/PVP samples calcined in air for 3 h with heating rate of 5 °C/min at different temperatures of (**a**) 500 °C, (**b**) 700 °C, and (**c**) 900 °C

increasing of calcination temperatures, indicating the enhancement of crystallinity due to the continuation of crystallization process and gradual grain growth [26]. The average crystallite sizes of the calcined LSMO samples were evaluated from X-ray line broadening of the reflections of (010), (104), (202), (024), (116), (214), (208) and (128). The crystallite size was estimated by Scherrer's equation (i.e., $D = K\lambda/(\beta \cos\theta)$, where λ is the wavelength of the X-ray radiation, K is a constant taken as 0.89, θ is the diffraction angle and β is the full width at half maximum (FWHM) [27]) and was obtained as 10 ± 4, 18 ± 8 and 33 ± 12 nm for the samples calcined at 500, 700, and 900 °C, respectively. This result shows that the crystallite size of the LSMO samples increases significantly with increasing the calcination temperature. The crystallite sizes are also summarized in Table 1.

Morphology and structure of the calcined LSMO samples were further characterized by TEM. Figure 5 shows bright field images with corresponding selected area electron diffraction (SAED) patters of the PVP/LSMO composite samples calcined at 500, 700, and 900 °C. It is clearly seen from the TEM bright-field images (Fig. 5) that the morphology and size of the materials were significantly affected by the calcination temperature. The 500 °C calcined sample remained as continuous structure with a fiber structure of ∼200 nm in diameter, whereas the 700 and 900 °C calcined with a fiber structure of packed particles or crystallites having particle sizes of 20–60 and 60–100 nm, respectively. It is worth noting that the particle size of LSMO contained in the 500 °C calcined sample is quite uniform. This might have resulted from the rates of hydrolysis involved in the fabrication process, in which the water required for the hydrolysis of metal precursors was supplied from the moisture in air [14–16]. Since the electrospun fibers were very small in diameter, the moisture could quickly diffuse into the fibers, causing a rapid and uniform hydrolysis of the metal precursors. This result is similar to that observed in electrospun $CoFe_2O_4$ nanofibers calcined at 500 °C [18]. The corresponding selected-area electron diffraction (SAED) patterns (Fig. 5) of all the PVP/LSMO composite nanofibers show

Table 1 Properties of the electrospun LSMO/PVP composites samples calcined in air for 3 h at 500, 700, and 900 °C

Calcination temperature (°C)	Crystal structure	Crystallite size (nm)	Saturation magnetization, M_s (emu/g)	Coercivity, H_C (Oe)
500	Rhombohedral	10 ± 4	1.23	13
700	Rhombohedral	18 ± 8	26.62	42
900	Rhombohedral	33 ± 12	40.52	54
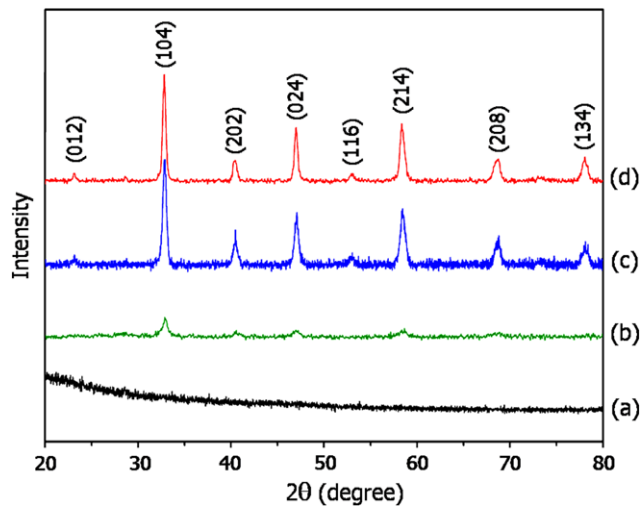
Fig. 4 XRD patterns of the as-spun LSMO/PVP and electrospun LSMO/PVP composite samples calcined in air for 3 h with heating rate of 5 °C/min

spotty ring patterns, revealing their crystalline rhombohedral structure. Increase in calcination temperature results in a stronger spotty pattern and the PVP/LSMO composite nanofibers calcined at 900 °C show strongest spotty patterns, indicating large crystallite of highly crystalline rhombohedral structure. Measured interplanar spacings ($d$hkl) from selected-area electron diffraction patterns in Fig. 5 are in good agreement with the values in the standard data (JCPDS: 51-0409).

The specific magnetization curves of the calcined LSMO samples obtained from room temperature VSM measurement are shown in Fig. 6. These curves are typical for a soft magnetic material and indicate hysteresis ferromagnetism in the field range of ±4500 Oe, while outside this range the specific magnetization increases with increasing field and tends to saturate in the field range investigated (±10 kOe). The specific saturation magnetization (M_s) values were obtained to be 1.23, 28.61, and 40.52 emu/g at 10 kOe for the LSMO samples calcined respectively at 500, 700, and 900 °C. It is found that the increase of the tendency of M_s is consistent with the enhancement of crystallinity, and the values of M_s for the calcined LSMO samples were observed to increase with increasing the crystallite size. It is noted that

the saturation values of 28.62 and 40.52 emu/g obtained in the LSMO samples calcined at 700 °C (crystallite size of 18–22 nm) and at 900 °C (crystallite size of 25–27 nm) are comparable to the reported values of 9.9–46.8 emu/g for the LSMO nanoparticles with crystallite size of 16–40 nm prepared by a simple thermal hydro-decomposition [28]. The increase in M_s for the calcined LSMO samples with increasing crystallite size may be explained by considering a magnetic domain of the samples [29]. Since the energy of a magnetic particle in an external filed is proportional to its particle size via the number of magnetic molecules in a single magnetic domain, the particle size will be increased and the crystallization will be more complete with increasing calcination temperature. Moreover, the magnetic phase will be increased because the perovskite structure is purer and more complete with the absorption of higher thermal energy. Thus, the larger particle or crystallite size leads to the higher value of the specific magnetization.

Figure 7 shows the plot of M_s versus $1/D$. It can be seen that M_s decrease linearly with increasing $1/D$. The linear decrease of M_s with the inverse of the crystallite size can be related according to the relationship [30]:

$$M_s(D) = M_s(\text{Bulk})\left(1 - \frac{\beta}{D}\right) \quad (1)$$

where $M_s(D)$ is the saturation magnetization of a sample with crystallite size D, $M_s(\text{Bulk})$ is the bulk saturation magnetization value, and β is a constant. It is seen from Fig. 8 that a slope is almost a straight line, confirming that the M values strongly depend on crystallite size. The ferromagnetic particles with diameter smaller than a critical size (D_C) have single magnetic domains such that their coercivity exhibits crystallite size dependence as expressed by the following equation [30]:

$$H_C = H_C^0\left(1 - \sqrt{\frac{D_P^3}{D^3}}\right) \quad (2)$$

where D_P is the upper limit of the crystallite size for superparamagnetic behavior with single magnetic domain, and H_C^0 is a maximum of H_C.

According to (2), for crystallite size larger than D_P, the magnetic moments of the single domain particles are

Fig. 5 TEM images with corresponding selected area electron diffraction patterns of the electrospun LSMO/PVP composite samples calcined in air for 3 h with heating rates of 5 °C/min at temperatures of (**a**) 500 °C, (**b**) 700 °C, and (**c**) 900 °C
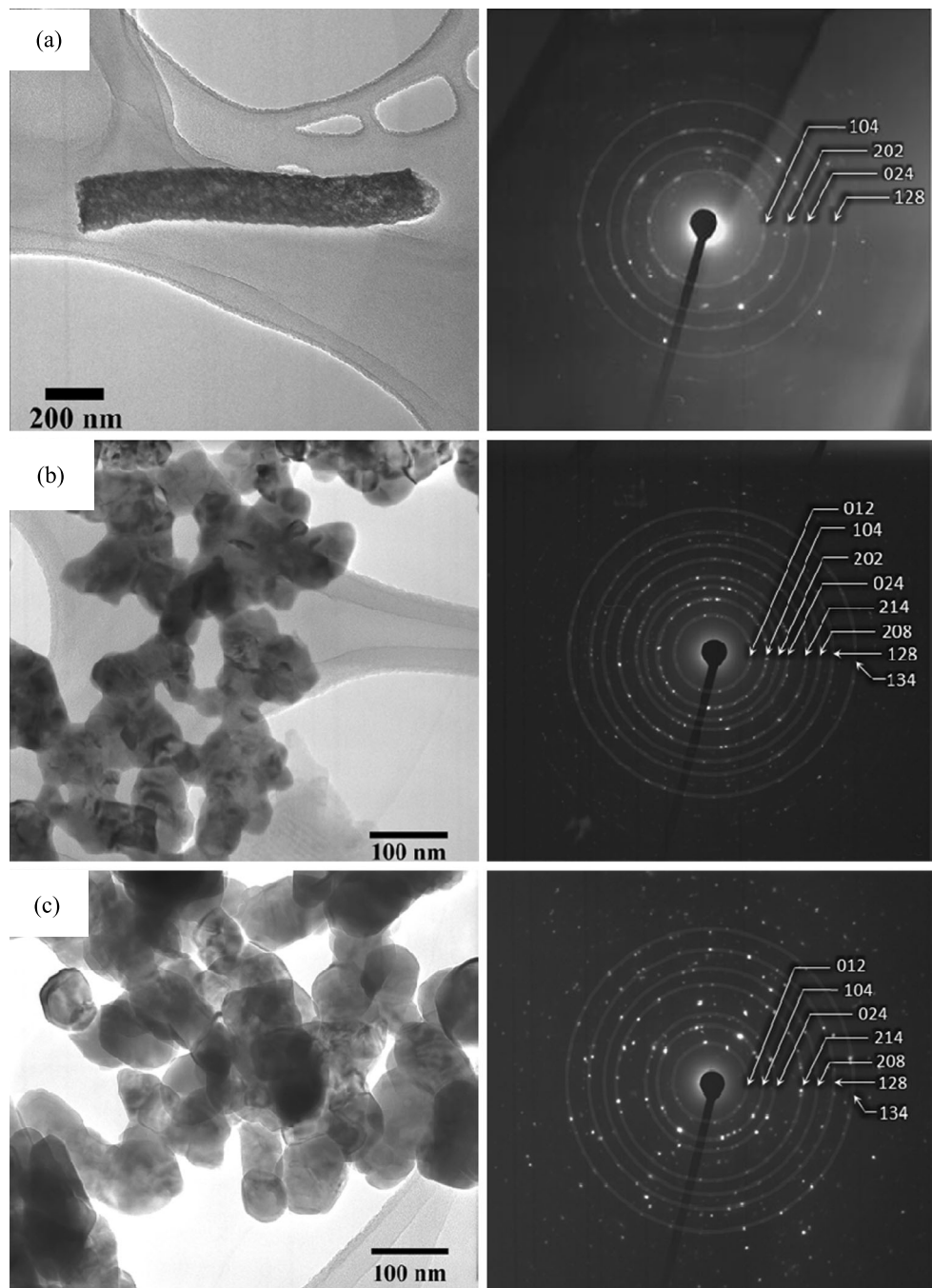
blocked and the H_C exhibits a $D^{-3/2}$ dependence until it reaches a maximum value of H_C^0 or the upper limit for single domain particle. The relationship between H_C and a function of $D^{-3/2}$ at room temperature is presented in Fig. 8.

From the linear portion of this curves, the maximum H_C (H_C^0) is obtained by calculating the intercept ion of H_C at the y axis, which results in $H_C^0 = 62$ Oe. Since from (2) the ratio H_C/H_C^0 is only a function of D, the values of H_C^0 can be thus used to normalize the plots of H_C and D as illus-trated in Fig. 9. The value of the crystallite size that makes the value of H_C/H_C^0 zero, or crystallite size having super-paramagnetic behavior can be calculated using the curvature of this graph. Since there are only three data sets, this cannot be calculated precisely. However, the observed trend of the curve can be assumed that the crystallite size about 10 nm or a calcined temperature about 500 °C is the condition caus-ing the superparamagnetic behavior of electrospun LSMO nanofibers.
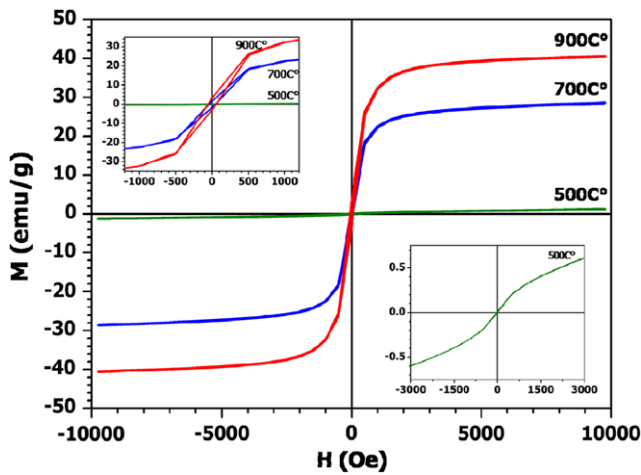
Fig. 6 The specific magnetization of the electrospun LSMO/PVP samples calcined in air for 3 h at 500, 700, and 900 °C, respectively, as a function of field, measured at 20 °C
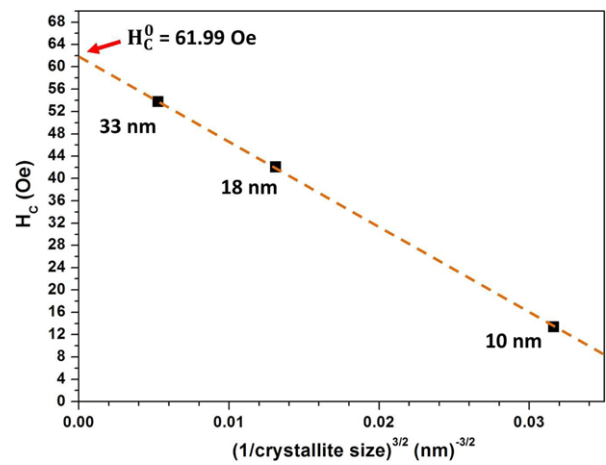

Fig. 8 Coercivity measured at room temperature for different average particle sizes as a function of $D^{-3/2}$ for the electrospun LSMO/PVP composite samples calcined at 500, 700 and 900 °C
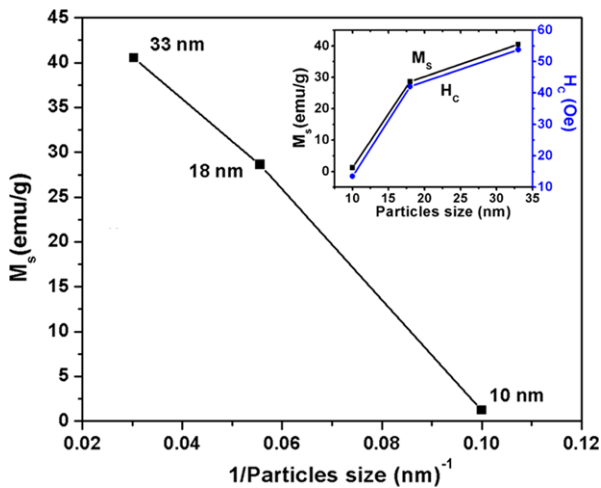

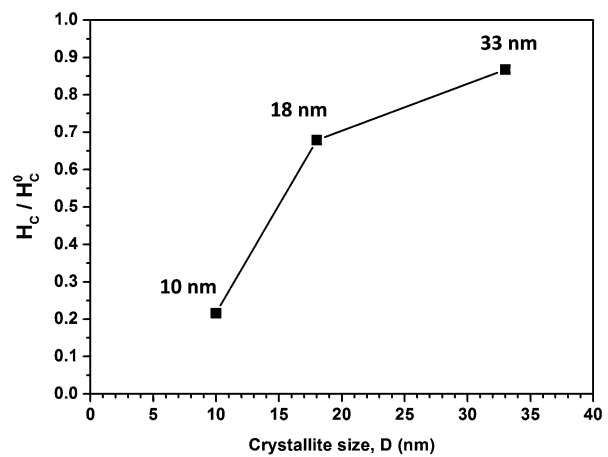**Fig. 7** The variation of magnetization and coercivity of the electrospun LSMO/PVP composite samples calcined at 500, 700, and 900 °C

Fig. 9 Normalized coercivity (H_C/H_C^0) as a function of the crystallite size for the electrospun LSMO/PVP composite samples calcined at 500, 700 and 900 °C

4 Conclusions

Nanostructures of LSMO have been successfully fabricated using electrospinning technique. After calcination of the as-spun (fiber size of 187 ± 41 nm in diameter) at 500–900 °C in air for 3 h with heating rate of 5 °C/min, LSMO nanostructures with packed particles or crystallite sizes of 11–27 nm having well-developed perovskite structure were obtained, as confirmed by XRD analysis. The crystal structure and morphology of the nanofibers were influenced by the calcination temperature. All the calcined samples of the LSMO nanostructures exhibited ferromagnetism. The specific saturation magnetization (M_s) values were obtained to be 1.23, 28.61, and 40.52 emu/g at 10 kOe for the LSMO samples calcined respectively at 500, 700, and 900 °C. We believe that the electrospun LSMO nanostructures would have potential in some new applications such as electrode materials in solid oxide fuel cells (SOFCs), gas sensors, membranes for separation processes, catalysts, electronic material for nanodevices and storage devices.

References

1. Helmolt, R.V., Wocker, J., Holzapfel, B., Schultz, M., Samwer, K.: Phys. Rev. Lett. **71**, 2331 (1993)
2. Balcells, L.I., Enrich, R., Mora, J., Calleja, A., Fontcuberta, J., Obradors, X.: Appl. Phys. Lett. **69**, 1486 (1996)
3. Wang, H., Zhang, X., Hundley, M.F., Thompson, J.D., Gibbons, B.J., Lin, Y., Arendt, P.N., Foltyn, S.R., Jia, Q.X.: Appl. Phys. Lett. **84**, 1147 (2004)
4. Bowen, M., Bibes, M., Barthélémy, A., Contour, J.P., Anane, A., Fert, A.: Appl. Phys. Lett. **82**, 233 (2003)
5. Desfeux, R., Bailleul, S., Costa, A.D., Prellier, W., Haghiri-Gosnet, A.M.: Appl. Phys. Lett. **78**, 3681 (2001)
6. Urishibara, A., Morimoto, Y., Arima, T., Asamitsu, A., Kido, K., Tokura, Y.: Phys. Rev. B **51**, 14103 (1995)
7. Bibes, M., Barthélémy, A.: IEEE Trans. Electron Devices **54**, 1003 (2007)
8. Jooss, Ch., Wu, L., Beetz, T., Klie, R.F., Beleggia, M., Schofield, M.A., Schramm, S., Hoffmann, J., Zhu, Y.: Proc. Natl. Acad. Sci. USA **104**, 13597 (2007)
9. Choi, S., Chung, M.-H.: Semin. Integr. Med. **1**, 53 (2003)
10. Hua, Z.H., Chen, R.S., Li, C.L., Yang, S.G., Lu, M., Gu, X.B., Du, Y.W.: J. Alloys Compd. **427**, 199 (2007)
11. Ji, G., Tang, S., Xu, B., Gu, B., Du, Y.: Chem. Phys. Lett. **379**, 484 (2003)
12. Huang, Z.H., Zhang, Y.Z., Kotaki, M., Ramakrishna, S.: Compos. Sci. Technol. **63**, 2223 (2003)
13. Reneker, D.H., Yarin, A.L., Fong, H., Koombhonge, S.: J. Appl. Phys. **87**, 4531 (2000)
14. Naunsing, S., Ninmuang, S., Jarernboon, W., Maensiri, S., Seraphin, S.: Mater. Sci. Eng. B **131**, 147 (2006)
15. Maensiri, S., Nuansing, W.: Mater. Chem. Phys. **99**, 104 (2006)
16. Maensiri, S., Nuansing, W., Klinkaewnarong, J., Laokul, P., Khemprasit, J.: J. Colloid Interface Sci. **297**, 578 (2006)
17. Li, D., Herricks, T., Xia, Y.: Appl. Phys. Lett. **8**, 4586 (2003)
18. Saengmanee, M., Maensiri, S.: Appl. Phys. A **97**, 167 (2009)
19. Ju, Y.-W., Park, J.-H., Jung, H.-R., Cho, S.-J., Lee, W.-J.: Compos. Sci. Technol. **68**, 1704 (2008)
20. Maensiri, S., Sangmanee, M., Wiengmoon, A.: Nanoscale Res. Lett. **4**, 221 (2009)
21. Ponhan, W., Maensiri, S.: Solid State Sci. **11**, 479 (2009)
22. Ponhan, W., Swatsitang, E., Maensiri, S.: Mater. Sci. Technol. **26**, 1298 (2010)
23. Zhou, X., Zhao, Y., Cao, X., Xue, Y., Xu, D., Jiang, L., Su, W.: Mater. Lett. **62**, 470 (2008)
24. Philip, J., et al.: J. Appl. Phys. **109**, 016109 (2011)
25. Zhi, M., Koneru, A., Yang, F., Manivannan, A., Li, J., Wu, N.: Nanotechnology **23**, 305501 (2012)
26. Mathur, S., Shen, H.: J. Sol-Gel Sci. Technol. **25**, 147 (2002)
27. Cullity, B.D., Stock, S.R.: Elements of X-Ray Diffraction, 3rd edn. Prentice-Hall, Englewood Cliffs (2001)
28. Daengsakul, S., Thomas, C., Thomas, I., Mongkolkachit, C., Siri, S., Amornkitbamrung, V., Maensiri, S.: Nanoscale Res. Lett. **4**, 839 (2009)
29. Daengsakul, S., Mongkolkachit, C., Thomas, C., Siri, S., Thomas, I., Amornkitbamrung, V., Maensiri, S.: Appl. Phys. A **96**, 691 (2009)
30. Sánchez, R.D., Rivas, J., Vaqueiro, P., López-Quintela, M.A., Caeiro, D.: J. Magn. Magn. Mater. **247**, 92 (2002)